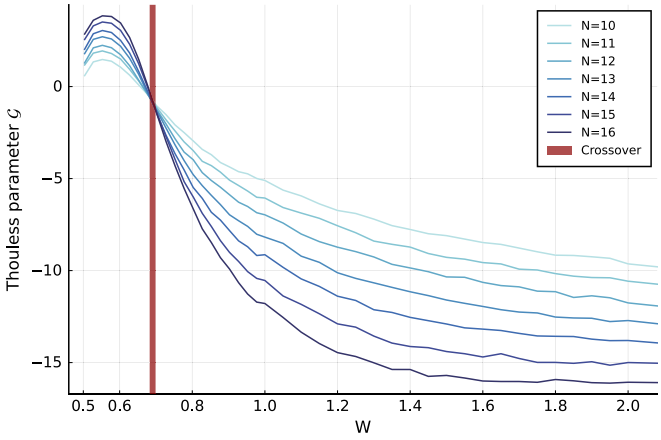

FIG. 3. Thouless parameter. Spectral and disorder averaged $\mathcal{G}$ versus disorder strength W. Data shown uses local operator $\hat{V}_1 = 2\hat{S}_z^{(1)}$

but couples the symmetry sectors only weakly, leading again to a very small energetic splitting of degenerate states. We want to emphasize the reason for level attraction being very different in nature in (I) and (IV): Whereas in (I) the system is close to a system with obvious conserved quantities due to symmetries, in (IV) there is the emergent integrability of the MBL regime [8]. Nevertheless, we expect region (I) to become less pronounced for larger systems continuing the trend visible in Fig. 2.

We conclude that, in analogy to standard MBL, we find a crossover in the level spacing distribution from a regime with level repulsion to Poissonian gaps indicating a localization crossover. At very strong disorder, we even find a region with level attraction, the source of which can be explained by the effective pair model.

B. Thouless parameter

Complementary to eigenvalue statistics, we also probe eigenstate properties by computing the Thouless parameter

$$\mathcal{G}_n = \ln \frac{|\langle n|\hat{V}|n+1\rangle|}{E'_{n+1} - E'_n}, \tag{4}$$

introduced by Serbyn *et al.* [53]. This quantity is akin to the Thouless conductance in single particle systems and quantifies how well two states $|n\rangle, |n+1\rangle$ with perturbed energies $E'_n = E_n + \langle n|V|n\rangle$ are coupled by a local perturbation $\hat{V}$. In the thermal phase, states of similar energy will have similar spatial structures, whereas in the localized phase, eigenstates are products of LIOM eigenstates and thus typically vary drastically from one to the next. One can derive the scaling of the average $\mathcal{G}$ in the thermal regime to be $\mathcal{G} \propto \log|\mathcal{H}|$ and in the localized regime to be $\mathcal{G} \propto -\log|\mathcal{H}|$, leading to the natural definition of the location of the crossover to be the point where $\mathcal{G} = \text{const}$ [53].

Figure 3 shows results using local operator $\hat{V}_1 = 2\hat{S}_z^{(1)}$. Data for local operators $\hat{V}_2 = 4\hat{S}_z^{(1)}\hat{S}_z^{(2)}$ and $\hat{V}_3 = \hat{S}_+^{(1)}\hat{S}_-^{(2)} + \text{H.c.}$ is visually identical. There is a very clear point where all curves intersect each other, indicating the crossover's location. To the right of the crossing point in the localized regime, the curves are roughly evenly spaced, reflecting the expectation of $\mathcal{G} \propto -\log|\mathcal{H}|$, clearly signaling the localized regime. The apparent absence of a drift of the transition point with system size is in contrast to observations in power-law interacting models with on-site disorder and will be further discussed in the next subsection.

C. Half-chain entropy

Having shown the presence of a localization crossover, we now demonstrate that our effective pair model is indeed a good approximation. We start by probing the half-chain entropy, $S = -\text{Tr}\rho_A \log_2 \rho_A$, with $\rho_A = \text{Tr}_B(\rho)$, i.e., the entanglement entropy between two halves of the chain. For that, we select $\lfloor \frac{N}{2} \rfloor$ consecutive spins and trace out the rest, resulting in two cuts due to the periodic boundary conditions, and average over all N possible choices of connected subsystems and all eigenstates.

In an ergodic system, all bulk states should exhibit volume-law entanglement, meaning $S \propto N$. In contrast, in a localized setting all states show area-law entanglement, which for $d = 1$ means $S = \text{const}$ [3,54].

To compute the half-chain entropy predicted by the pair model, we need to determine how many pairs are divided by each cut and how often these pairs are found in one of the entangled states $|\pm\rangle = 1/\sqrt{2}(|\uparrow\downarrow\rangle \pm |\downarrow\uparrow\rangle)$. Not all pairs consist of adjacent spins [see Fig. 1(c)], so a cut can separate more than one pair. The amount of cut bonds is easily determined from the position data alone by adding up the distances between paired spins. Respecting periodic boundary conditions of the system yields an additional factor of 2, since there are two cuts needed to divide the chain.

Considering the entropy contribution of a single bond, if we were to average over all possible configurations of pair states, each cut bond would contribute half a bit of entanglement on average, as half of the pair states are maximally entangled and the other half not entangled at all. However, here we consider the sector of smallest positive magnetization, which yields a slightly larger entropy, because it favors the entangled states $|\pm\rangle$ (which have zero net magnetization) over the fully polarized ones. This modification can be computed exactly (see Appendix B for details).

Taking into account both the effects of extended pairs and of the fixed total magnetization, we can compute a prediction for the entanglement entropy directly from the interaction matrix J_{ij}. Figure 4 shows both the numerically computed values for different system sizes (solid) and pair-model prediction (dashed).

We clearly see the change between the ergodic and localized regime for the numerically computed data. For strong disorder, all lines collapse, confirming on one hand the area law entanglement expected in the localized phase and, on the other hand, validating the pair model as it predicts the strong-disorder limit with high accuracy. Figure 4(b) magnifies the strong-disorder regime showing that the pair-model prediction in fact slightly overestimates the half-chain entropy for very strong disorder. This might indicate that there are spins that do not pair up perfectly, not forming a maximally entangled Bell pair. It is plausible that this happens at late stages of the